PHYSICAL REVIEW B **82**, 035401 (2010)

# Frictional duality of metallic nanoparticles: Influence of particle morphology, orientation, and air exposure

Dirk Dietzel,[1] Tristan Mönninghoff,[1] Carina Herding,[1] Michael Feldmann,[1] Harald Fuchs,[1] Bert Stegemann,[2] Claudia Ritter,[3] Udo D. Schwarz,[3] and André Schirmeisen[1,*]

[1]*Physikalisches Institut and Center for Nanotechnology (CeNTech), Westfälische Wilhelms-Universität Münster, D-48149 Münster, Germany*

[2]*University of Applied Sciences (HTW) Berlin, D-12459 Berlin, Germany*

[3]*Department of Mechanical Engineering and Center for Research on Interface Structures and Phenomena (CRISP), Yale University, New Haven, Connecticut 06520-8284, USA*

(Received 21 February 2010; revised manuscript received 25 May 2010; published 1 July 2010)

The contact area dependence of the interfacial friction experienced during the translation of antimony nanoparticles deposited on a graphite substrate is studied under different conditions using the tip of an atomic force microscope as a manipulation tool. In vacuum a dual behavior of the friction-area curves is found, characterized by the observation that some particles exhibit friction below the detection limit while other similarly sized particles showed constant shear stress values. Detailed investigations prove the reproducibility of this effect, revealing that neither the particle's morphology nor their alignment relative to the substrate lattice influence the findings. In contrast, we observe that a temporary exposure to ambient air can lead to a drastic increase in the particle's friction.

DOI: 10.1103/PhysRevB.82.035401 PACS number(s): 07.79.Sp, 46.55.+d, 81.40.Pq, 61.46.Df

## I. INTRODUCTION

Nanotribology has become a field of fast growing interest in the recent years.[1] Research has been spurred not only by a fundamental interest in understanding the basic physical laws of friction on the nanoscale, but increasingly also by pressing technological challenges related to the accelerated pace of miniaturization in MEMS and NEMS technology. In fact, the functionality of nanodevices with moving parts is largely limited by friction-related wear effects, as classical lubrication methods fail on the nanometer scale. The development of new strategies, on the other hand, requires a thorough understanding of nanoscale friction.

A particularly useful tool for studying nanoscale friction is the friction force microscope,[2] a variant of the atomic force microscope[3] that allows the simultaneous measurement of topographical data and lateral forces. Friction force microscopy (FFM) has been employed in numerous studies since its invention in 1987, including work aimed at mapping nanoscale friction,[4,5] analyzing the atomic-scale origin of friction,[2,6–9] or even controlling friction.[10,11]

Despite its success, there are inherent limitations to friction force microscopy. For example, analysis of the contact area dependence of nanoscale friction by FFM has been problematic, as the contact area between tip and sample cannot be varied easily. One solution has been the controlled preparation of FFM tips with different apex radii,[12,13] a tedious and rarely used procedure. Commonly, the contact area has been changed by simply varying the cantilever load and thus inducing contact area changes by surface deformations. Although different contact models[14–17] have been applied to describe the experimentally observed relation between load, contact area, and friction,[12,13,18,19] this approach suffers typically from the limited knowledge about the exact geometry of the tip. Moreover, inducing stress at the interface might affect the system's frictional properties, making it difficult to distinguish between stress-related and contact area-related effects. Finally, FFM is also limited regarding the possible choice of material combinations. Probe tips usually consist of silicon or related materials such as silicon nitride and silicon oxide, which defines already one component of the interface. An additional impediment in this regard is that the atomic structure of the probe tips is generally ill defined, which complicates systematic measurements.

To overcome the above-listed limitations, combinations of FFM with nanoparticle manipulation have recently been developed. Traditionally, atomic force microscopy (AFM) based manipulation of nano-objects focused on the exact positioning of particles[20–23] as well as the characterization of the factors that govern the tip-imposed particle movement.[24–29] A new route toward understanding nanoscale friction[30] has then been opened by quantifying the interfacial friction between the nanoparticle and the substrate during the manipulation process, which enables the study of the frictional behavior for a wide variety of material combinations with well-defined interface conditions.[31–36] Under ultrahigh vacuum (UHV) conditions nanoparticles can be manipulated on clean, atomically flat substrates, allowing the investigation of the atomic origins of friction for extended contacts. By using appropriate substrates and particles, it is even possible to study the influence of crystallographic structure and orientation.

A further advantage of such manipulation studies is that a large number of similar particles can be examined easily, which is difficult to achieve in conventional FFM experiments. While this strengthens conclusions by large statistics, values reported in such studies might still depend on the specific interface conditions including the level of contamination, the presence of surface defects, or nonuniform structural or morphological properties of the particles.

The present work aims at providing such additional information for the model system of metallic antimony nanopar-

 

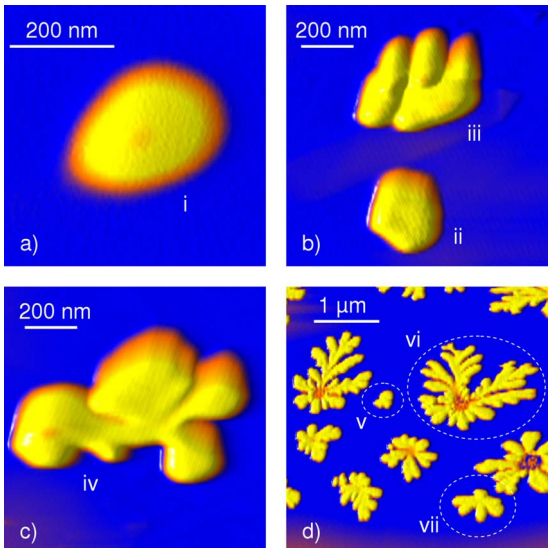


FIG. 1. (Color online) Evolution of particle morphology with size. The contact areas of the particles shown in (a)-(d) are (i) 60 000 $nm^2$, (ii) 66 000 $nm^2$, (iii) 135 000 $nm^2$, (iv) 360 000 $nm^2$, (v) 60 000 $nm^2$, (vi) 1 180 000 $nm^2$, and (vii) 240 000 $nm^2$. While smaller particles are usually round and compact (e.g., particles (i), (ii), larger particles perform a transition to more complex branched structures (e.g., particle (vi). The color scale ranges from 0 nm (dark blue) to ≈60 nm (bright yellow).

ticles evaporated on highly oriented pyrolytic graphite (HOPG) substrates under UHV conditions. This model system has previously been studied,[26,32,34,36,37] revealing a "frictional duality" where some particles show finite friction while for others, friction appears to vanish. Investigating the physical origin of this duality in more detail, it has been found that neither the particle morphology nor the sliding direction affect friction significantly, while oxidation can cause dramatic changes.

## II. EXPERIMENTAL

### A. Nanoparticle preparation and sample characterization

The samples under investigation consisted of antimony nanoparticles prepared by thermal evaporation on HOPG substrates. Unless otherwise noted, the HOPG was cleaved under UHV conditions directly before thermal evaporation, which was carried out by heating the crucible to 370 °C for 20 min while leaving the substrate at room temperature. Using these parameters, nanoparticles with a wide range of surface area sizes could be prepared. Typically, antimony nanoparticles show different types of structures depending on their surface area.[38] This is illustrated in Fig. 1, where AFM images show the three basic categories of nanoparticles that are encountered: A) Small nanoparticles, which are mostly round and compact [Figs. 1(a), 1(b), and 1(d), particles i, ii, and v]; B) larger nanoparticles starting to show the onset of branching [Figs. 1(b)–1(d), particles iii, iv, and vii]; and C) very large nanoparticles with complex branched morphologies [Fig. 1(d), particle vi]. In general, for nanoparticles produced by the evaporation conditions described above, the compact structure was found to be predominant for nanoparticles of up to 100 000 $nm^2$ with only larger nanoparticles showing branched structures. Interestingly, large fluctuations of contact area dimensions can be found already on small sections of the substrate [cf. Figure 1(d)]. Experiments presented in this work, however, were limited to nanoparticles belonging to categories A or B with surface areas smaller than 200 000 $nm^2$.

The morphological transition from round to branched was already observed in earlier work[38,39] and reported to coincide with structural changes in the particle's crystalline structure: While the small, compact particles are amorphous, it was found that the larger, branched nanoparticles are crystalline. The crystalline structure of large particles is confirmed by our high-resolution *in situ* FFM measurements shown in Fig. 2. The measurements, which have been performed on top of a particle with a particle-substrate contact area of $A_{contact}=120\ 000\ nm^2$, yielded stick-slip behavior [Figs. 2(a) and 2(c)] with a periodicity of $(0.41\pm0.04)$ nm that matches well with the lattice constant of hexagonal antimony (0.43 nm).[40,41] In contrast, no regular stick-slip pattern was found for any of the smaller round islands, which are expected to be amorphous.[38] In order to determine the lattice orientation of the substrate we also carried out similar high-resolution FFM imaging directly on the graphite surface, where regular stick-slip behavior was found as well [Figs. 2(b) and 2(d)].

In Fig. 3, we show transmission electron microscopy (TEM) measurements of the Sb particles to further investigate the amorphous-crystalline transition in relation to the observed morphology changes from small and compact to large and branched. For small and round nanoparticles [Fig. 3(a)], selected area electron diffraction (SAED) shows no diffraction pattern, but rather a homogenous, diffuse signal [Fig. 3(b)], which indicates that the particles are indeed amorphous. For the larger and branched nanoparticles [Fig. 3(c)], however, a distinct diffraction pattern can be observed [Fig. 3(d)], confirming their crystalline structure.

### B. Particle manipulation and friction calibration

All experiments have been performed at room temperature under UHV conditions using a commercial Omicron AFM/STM combination. The base pressure during both evaporation and manipulation was approximately $5\times10^{-10}$ mbar and the samples were transferred from the preparation chamber to the analysis chamber without breaking the vacuum.

To assess the interfacial friction between the nanoparticles and the HOPG substrate, we employed an AFM-based particle manipulation scheme that has been described in detail elsewhere.[37] In short, the friction measurements have been performed by pushing the nanoparticles from the side as illustrated in Fig. 4 while operating the instrument as a conventional friction force microscope using soft Si or SiN cantilevers with normal force constants of up to $k=0.3$ N/m. During the nanoparticle movement, an increased torsional signal is measured that can be identified as the additional interfacial friction between nanoparticle and substrate.[31,37] In order to obtain quantitative results, all measurements have

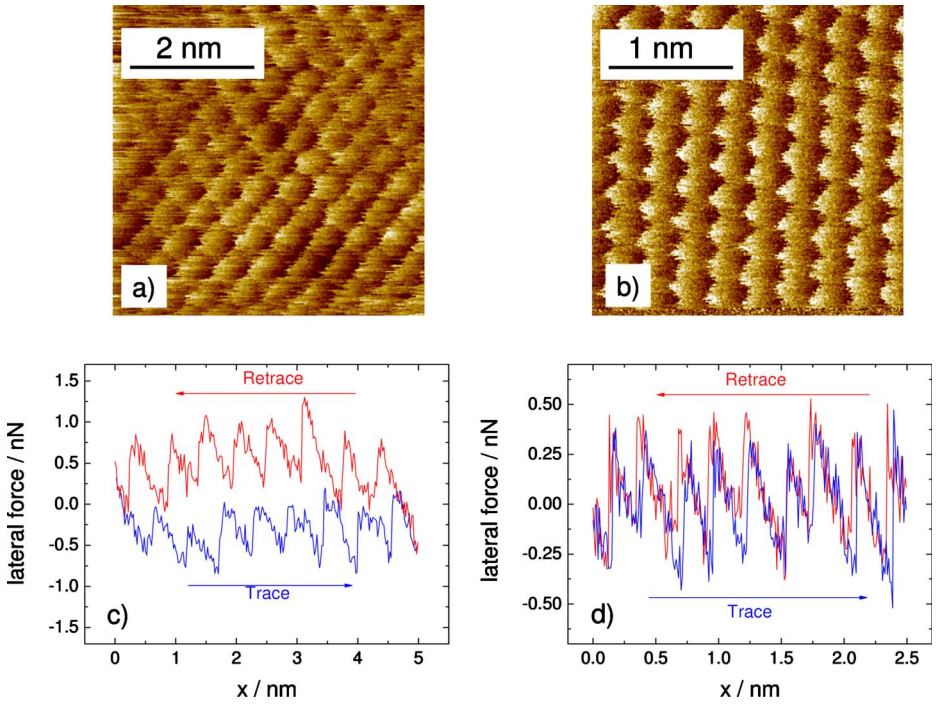


FIG. 2. (Color online) Conventional friction force microscopy performed on top of a large Sb nanoparticle with $A_{\text{contact}}=120\ 000\ \text{nm}^2$ (a; image size: $5\times5\ \text{nm}^2$) and the adjacent HOPG substrate (b); $2.5\times2.5\ \text{nm}^2$). Additionally, friction loops measured along the fast scan axis are shown for both the antimony nanoparticle (c) and the HOPG substrate (d). In both cases, the lateral force signals show regular stick-slip behavior.

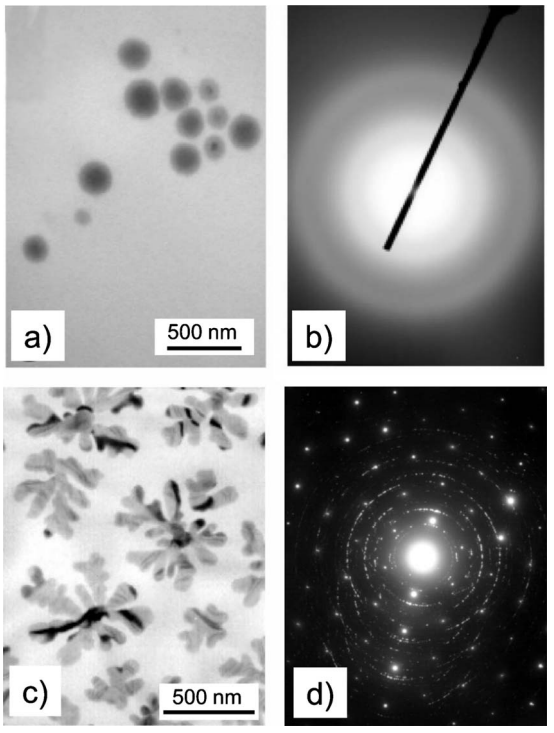


FIG. 3. Structural analysis of antimony nanoparticles. (a) TEM measurements performed on small and round nanoparticles. (b) Selected area electron diffraction of the nanoparticles shown in (a). (c) and (d) TEM (c) and SAED (d) measurements of larger, branched nanoparticles.

been calibrated using the wedge calibration method described by Varenberg *et al.*[42]

The manipulation process is controlled by adjusting the normal force exerted by the cantilever during scanning; while low-normal forces of $\approx1$ nN enable regular imaging, forces of above 20 nN typically induce nanoparticle movement.[37] By adjusting the normal force close to the threshold of manipulation, particles of a certain size are likely to be moved during the scan process while larger particles remain stationary.

An example of a manipulation event based on this approach is presented in Fig. 5. Figure 5(a) shows a topographic image of a nanoparticle with $A_{\text{contact}}=48\ 000\ \text{nm}^2$ directly before the manipulation. In the subsequently recorded image displayed in Fig. 5(b), the nanoparticle seems to be "cut" after some part has been imaged. In fact, the particle was pushed by the AFM tip out of the view of sight along the line indicated by the white dashed arrow. Figure

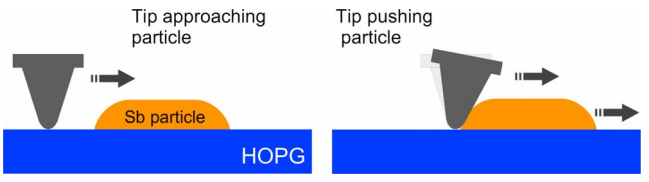


FIG. 4. (Color online) Schematic of the manipulation process. Left: The AFM tip, which profiles the substrate in contact mode, approaches the nanoparticle. Right: The probe tip reaches the nanoparticle and pushes it along its scan path. An increased cantilever torsion is observed due to the additional lateral force acting on the tip during the nanoparticle translation.

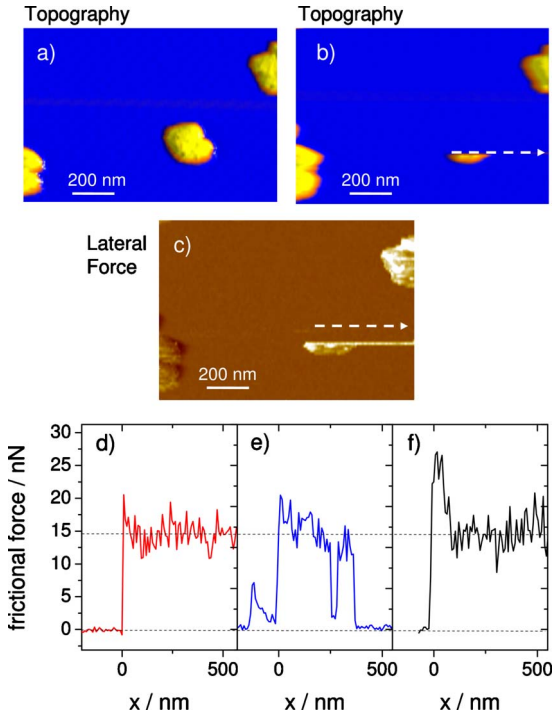


FIG. 5. (Color online) Example of a particle manipulation event. (a) A small nanoparticle with $A_{contact}$=48 000 nm$^2$ is imaged using a low cantilever load. (b) Exerting a higher load causes manipulation of the nanoparticle. After the nanoparticle has been profiled by the AFM tip for a few lines in this bottom-to-top scan, it is pushed along the line indicated by the white dashed arrow and ultimately removed from the field of view. (c) Lateral force signal acquired simultaneously with the topographical data shown in (b). The increased lateral force due to the nanoparticle manipulation is clearly visible. (d) A quantitative interfacial friction value can be extracted by analyzing the scanline at which manipulation occurred. The interfacial friction is calculated from the difference between the average lateral force signal before and during manipulation. The same nanoparticle was manipulated two more times (e) and (f) with very similar results.

5(c) shows the corresponding friction force image simultaneously acquired with the topographic image of Fig. 5(b), which features a pronounced straight line along the path of the particle translation.

This "friction trace," which can be identified as the lateral force signal during the particle movement, is depicted in detail in Fig. 5(d). At the position $x$=0, the tip hits the nanoparticle and a sudden increase of the friction signal is observed compared to the reference level defined by the friction between the AFM tip and the HOPG substrate, which was set to zero. The lateral force signal then remains constant at a level of about 15 nN throughout the recorded manipulation path. In Figs. 5(e) and 5(f) the friction signals of two further manipulations of the same particle are shown. For all three successive manipulations, no significant variations of the measured interfacial friction force could be observed during the effective translation length of approximately 1.5 $\mu$m, demonstrating the reproducibility of the approach.

### C. Contact area determination

One of our main motivations for performing the present friction measurements by particle manipulation techniques is to analyze the contact area dependence of nanoscale friction. For this it is important to precisely determine the true interface area of the sliding contact $A_{contact}$. Based on energy minimization arguments, it is reasonable to assume that an atomically flat contact between the antimony nanoparticles and the HOPG substrate is established during growth. This assumption is corroborated by cross-sectional TEM images to be presented in a forthcoming publication,[43] which show that thermally evaporated antimony nanoparticles form a flat interface with the HOPG substrate. Therefore, it can be expected that the apparent nanoparticle-substrate contact area from AFM topography scans correctly represents the true contact area. For the analysis of the present experiments, this area has been approximated by drawing polygons around the nanoparticle circumferences that closely follow the particle edges when depicted as two-dimensional top views. The area of the polygon is then a measure of the nanoparticle's contact area.

## III. RESULTS

### A. Contact area dependence of friction

In our previous study,[34] we found two coexisting frictional states for Sb nanoparticles: While some particles showed finite friction that increased linearly with the interface area and allowed to deduce an area-independent shear stress of $(1.04 \pm 0.06)$ nN/nm$^2$, other particles assumed a state of frictionless ("superlubric") sliding.[44] This "frictional duality" is illustrated in Fig. 6, which shows the topographical (top row) and frictional (bottom row) signals of three consecutive scans. The topographical image Fig. 6(a) was used to determine the contact area of the two particles with the substrate (note that both particles appear to consist of smaller particles that coalesced during growth). The corresponding friction map [Fig. 6(d)] was acquired simultaneously with the topographical data of Fig. 6(a) and features strong contrast at the edges of the particles, a commonly known artifact of FFM.

Directly after completing the scan of Fig. 6(a), the topographical image displayed in Fig. 6(b) has been recorded with a normal force set slightly above the threshold force expected to initiate particle dislocation. As a result, the upper particle is moved out of the field of view after being profiled for only a few scan lines, while the lower particle remains in its original position. For the upper particle, lateral forces during dislocation [Fig. 6(e)] are only visible before it is moved (note the small bump close to the upper end of the image, which correspond to the topographic edge visible in Fig. 6(b); no lateral force signal can be detected during the actual particle sliding ["vanishing friction event," see Fig. 6(g)].

Figure 6(c) presents the image subsequent to Fig. 6(b), with Fig. 6(f) showing the accompanying lateral force signal. This time, the lower particle is pushed out of the field of view after it has been mapped for a couple of scan lines. Since the dislocation of the lower particle involves continu-

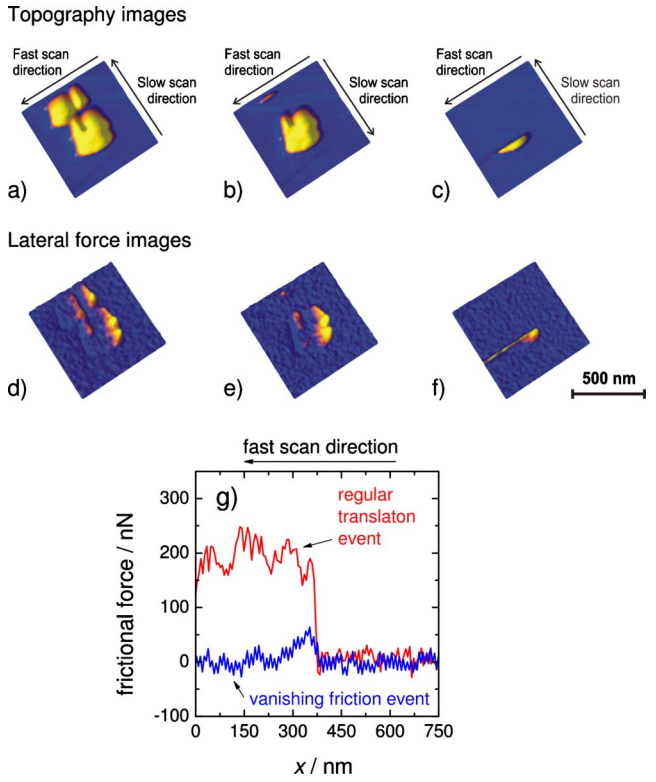


FIG. 6. (Color online) Topography signals (top row) and lateral force signals (bottom row): (a) and (d) measured before particle dislocation, (b), (c), (e), (f) measured during the dislocation of two nanoparticles. (b), (e): dislocation of upper particle with $A_{\text{contact}} = (60\,000 \pm 5000)$ nm$^2$; (c), (f): dislocation of lower particle with $A_{\text{contact}} = (84\,000 \pm 5000)$ nm$^2$. (g) Direct comparison of the respective lateral force signals during particle dislocation. While the red curve, corresponding to the event depicted in (c) and (f), shows considerable finite friction (labeled in the figure as "regular translation event"), no apparent friction other than a small initial sticking is visible for the blue curve representing the translation of the particle pushed in (b) and (e).

ously applied lateral forces, an apparent "tail" manifests in Fig. 6(f). The analysis of the lateral forces recorded during each particle translation [Fig. 6(g)] allows us to quantify the occurring frictional forces. The distinct frictional signature of the lower particle is in striking contrast to the virtually frictionless sliding of the upper particle, representing a good example for "frictional duality" observed within one scan frame.

A summary of our complete friction vs contact area data is presented in Fig. 7, where results of manipulation experiments with nanoparticles sized from 7000 nm$^2$ to 200 000 nm$^2$ are shown. First we discuss the filled symbols, which represent measurements carried out on particles that were prepared and analyzed under clean UHV conditions and never left the vacuum chamber. For these particles, the frictional duality manifests between the filled black and red symbols: The black symbols reflect interfacial friction values that can be approximated by the area-independent shear stress of $\approx 1.04$ nN/nm$^2$ found earlier,[34] while the red symbols characterize superlubric events.

As a possible explanation for this duality, it has been proposed that interface contamination due to mobile spacer molecules might mediate friction between incommensurate (and thus superlubric) interfaces.[45–48] This line of argument is motivated by the fact that even under UHV conditions some interface contamination occurs over time, in particular for samples that are stored for an extended period of time after preparation. Therefore, two series of measurements have been performed. In a first series, all manipulations were conducted within approximately two months, whereas a second series was performed within a minimum time span after sample preparation ($<2$ days). Additionally, the HOPG substrate was cleaved under UHV conditions for the second series, while in the first case the HOPG was cleaved in air (both samples were heated *in situ* after cleavage). By implementing these changes, which are expected to improve sample cleanliness, the ratio of superlubric to nonsuperlubric particles was indeed found to increase.[34]

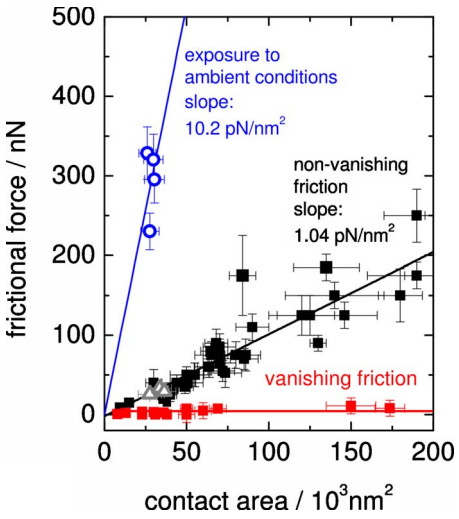


FIG. 7. (Color online) Interfacial friction force vs. contact area measured for Sb nanoparticles manipulated on an HOPG substrate. All measurements have been performed under UHV conditions. The full markers (squares) represent unoxidized nanoparticles kept permanently under UHV conditions. These particle show either a constant, finite shear stress (black), or vanishing friction (red). The open symbols (triangles and circles) represent Sb nanoparticles that had been exposed to ambient conditions prior to the friction measurements. Note that the triangles (gray) are located on the branch of finite shear stress, while the circles (blue) form a second branch of high shear stress.

Even though these findings seem to support the above arguments, caution is still advised. In general, the actual ratio of the number of particles showing vanishing friction to the ones featuring nonvanishing friction is difficult to determine and might be higher than concluded from the present experimental results ($\approx 1:4$). This is because the measurement procedure relied on contact mode operation for initial imaging, which inherently favors the detection of nonvanishing friction particles. In this regard, using the dynamic imaging mode instead would assist the establishment of a more accurate ratio.

In our previous study,[34] vanishing friction events were only observed up to a maximum size of 90 000 nm$^2$, raising the issue whether an upper limit for superlubric sliding exists. Our newer measurements revealed the existence of van-

ishing friction particles for the entire range of contact areas investigated, with superlubric events recorded for particle sizes of up to 180 000 $nm^2$ (Fig. 7). One can therefore speculate that there might be no upper limit for superlubric sliding as long as atomically flat, clean, and sufficiently rigid interfaces can be created.

### B. Effect of particle oxidation

In a next set of experiments, we have analyzed antimony particles exposed to air, which is known to cause surface oxidation.[34] Specifically, Sb nanoparticles prepared in UHV (HOPG cleaved in air and heated *in situ* after cleavage) were removed from the vacuum chamber and kept under ambient conditions for approximately two weeks. The sample was then reinserted into the vacuum chamber, heated to 150 °C for about 1 h in order to remove adsorbed water, and subsequently transferred to the UHV AFM where the particles were manipulated as before. Interestingly, the friction values observed for these particles (open symbols in Fig. 7) can again be divided into two levels: The "lower level" (open gray triangles) is in good agreement with the nonvanishing friction branch measured for non-air-exposed particles, while the "upper level" shows a roughly ten times higher interfacial friction, resulting in an effective shear stress of $(10 \pm 3)$ $pN/nm^2$. In these experiments, no particles were found to fall onto the vanishing friction branch after air exposure.[49]

A shear stress of air-exposed Sb nanoparticles on HOPG that is much higher than for clean particles under UHV conditions has been reported before.[34] The difference between the value found in these earlier experiments (40 $pN/nm^2$) and the present value may stem from additional surface contamination such as adsorbed water, as the earlier experiments were performed under ambient conditions. Systematic errors in the absolute friction calibration may also play a role, since different AFM systems were used.

Numerous scenarios may be envisioned to explain the observed change of friction as a result of the air exposure. For example, all vanishing friction particles might switch to the very high friction branch while particles initially exhibiting nonvanishing friction might be unaffected by air exposure. Another possibility is that all particles from the nonvanishing friction branch oxidize yielding a ten times higher frictional resistance while all particles showing vanishing friction undergo an air-induced transformation that coincidentally results in frictional values coinciding with the nonvanishing friction branch found in UHV.

Most of the theoretically possible scenarios, however, appear to be improbable for one or the other reason. Based on the currently available information, we favor a scenario where at least some of the nonvanishing friction particles change their frictional properties from the 1 $pN/nm^2$ to the 10 $pN/nm^2$ branch due to air exposure while others remain unaffected. Further, we found no vanishing friction particles on the oxidized sample suggesting that the vanishing friction branch is completely lost by the long-term air exposure. Despite the low statistics, this seems reasonable in light of our previous observation that the ratio of vanishing to nonvanishing friction particles increases with the level of clean UHV sample preparation.

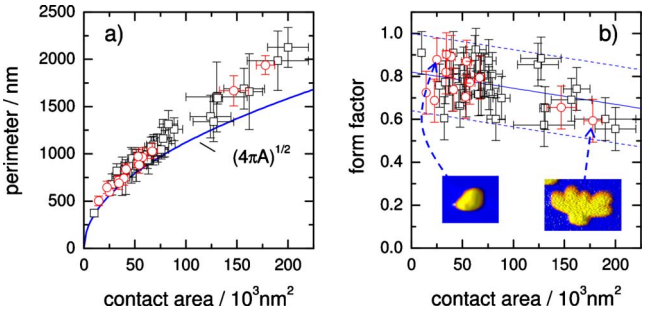


FIG. 8. (Color online) Perimeter (a) and form factor $\gamma_{form}$ (b) plotted vs nanoparticle contact area with round red markers for particles featuring low friction and square black markers for high friction particles. The solid blue curve in (a) indicates the theoretical lower limit of perimeter for perfectly round particles. The two AFM images used as inset in (b) illustrate the particle shapes for different form factors (left particle: $A_{contact}=25\ 000\ nm^2$, $\gamma_{form}=0.88$; right particle: $A_{contact}=178\ 000\ nm^2$, $\gamma_{form}=0.59$).

To explain the appearance of the "very high friction" branch, we argue that oxidation proceeds in these cases into the Sb-HOPG interface although it is not directly exposed to air. The fact that some air-exposed particles seem to remain on the high friction branch of the unexposed particles indicates on the other hand that not all interfaces are affected by the assumed oxidation process. Rather, oxidation may need a seed defect to proceed all the way into the Sb-HOPG interface, which may not be present in all cases. Independent of the exact scenario, we emphasize that air exposure of Sb nanoparticles on HOPG can lead to an increase of the interfacial friction by one order of magnitude, an unexpectedly strong influence.

### C. Effect of particle morphology

The discussion in Sec. II A showed that the growth of Sb nanoparticles is a complex process where particle shapes varying from almost round to very branched can be obtained. It is therefore obvious to suspect an influence of the particle morphology on its frictional properties. In order to quantify morphological differences we have analyzed the relation between particle perimeter and contact area.[50] Furthermore we calculated a "form factor" $\gamma_{form}$ defined as

$$\gamma_{form} = \frac{4 \cdot \pi \cdot A_{contact}}{L^2_{perimeter}}. \quad (1)$$

Equation (1) yields $\gamma_{form}=1$ for perfectly round particles whereas any deviation from circular shape results in form factors smaller than one.

Figure 8 shows both the perimeter and the form factor as function of the contact area for particles showing high and low friction (black squares and red circles, respectively). Particles exposed to air were not included in this analysis. The blue curve in Fig. 8(a) represents the theoretical perimeter for perfectly round samples, which represents the lower limit for all data points at a given contact area, while in Fig. 8(b)

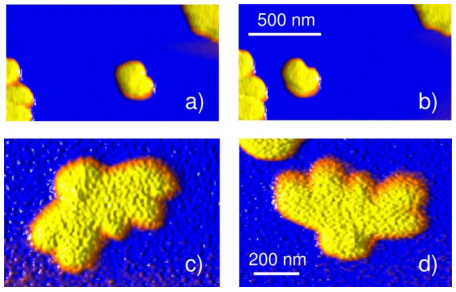


FIG. 9. (Color online) Examples of particle rotations occurring during the manipulation of antimony nanoparticles. In (a) and (b), the same nanoparticle as featured earlier in Fig. 5 is displayed before the first (a) and before the third (b) manipulation with an effective rotation of $\cong 15°$, whereas the nanoparticle imaged in (c) and (d) is shown at the start (c) and after completion (d) of a series of multiple manipulations ($n>10$) that resulted in an accumulated rotation of $\approx 135°$.

a range of typical form factors distribution is indicated by straight lines to guide the eye.

From Fig. 8(a), we see that the measured particle parameters stay close to the theoretical curve for small contact areas, whereas large contact areas result in a growing discrepancy from the theoretical curve. This is consistent with the decreasing form factors for larger contact areas in Fig. 8(b), where nanoparticles appear to be randomly distributed within a range of approximately $\pm 0.15$ around the center, and simply reflects our earlier finding of increased branching for larger particles. However, as particles showing either high or low (vanishing) friction are dispersed in the same way, a direct correlation between particle morphology and frictional properties, i.e., superlubric or not, can be excluded.

### D. Effect of particle rotation

As an alternative to the "dirt particle" theory,[45,46] it has been suspected that a relative rotation of the atomic lattices of surface and particle may be responsible for the frictional duality. This mechanism was proposed by Dienwiebel *et al.*,[51] where the registry between a small graphite flake sliding on a single-crystalline graphite substrate was found to strongly influence friction. In their experiments, Dienwiebel *et al.* found high values for graphite-graphite friction always when the relative orientation between HOPG substrate and graphite flake yielded commensurate interface conditions, while friction vanished otherwise. To evaluate a possible influence of the relative lattice orientations for the present system, we have manipulated selected nanoparticles multiple times and analyzed the results with respect to the particle-substrate alignment.

Figure 9 features two examples of particle rotation. In Figs. 9(a) and 9(b) we show the same antimony nanoparticle with $A_{\mathrm{contact}}=48\ 000\ \mathrm{nm}^2$ that has been discussed earlier in Fig. 5 (referred to as the "small particle" in the following), which is rotated modestly by about 15° during manipulations. In contrast, Figs. 9(c) and 9(d) illustrate that rotations can also accumulate to larger values: We performed multiple successive manipulations ($n>10$) with this "large particle" ($A_{\mathrm{contact}}=178\ 000\ \mathrm{nm}^2$), which actually resulted in a relative rotation of $\alpha \approx 135°$.

In the case of rotation dependent commensurability, this "large particle" should lock at least at some point during these rotations into commensurate conditions that cause much higher friction (note that the particle is expected to be crystalline due to its large size). However, during all manipulations performed, the large particle's friction level remained on the vanishing friction branch, strongly disfavoring the hypothesis that lattice structure matching causes the observed frictional duality. This is further corroborated by multiple manipulations of the "small particle" shown in Figs. 9(a) and 9(b), which features non-vanishing friction. Again, no variations in interfacial friction have been observed (cf. Figures 5(d)–5(f)) for different rotation angles despite the fact that even moderate rotations should be sufficient to alter the particle's frictional properties if the structure-matching hypothesis would apply.

While studying rotational effects we also revisited the question whether friction depends on the contamination level of the nanoparticle/substrate system by modestly increasing the pressure inside the UHV chamber after a first run of rotation experiments had been completed. This was achieved by switching off the vacuum pumps and shortly opening a fine dosing valve to contaminate the UHV with ambient air, which resulted in a pressure increase from $p_0=5\times 10^{-10}$ to $p_1=5\times 10^{-5}$. The chamber containing the AFM and the sample was then kept at $p_1$ for 30 min before starting the pumps again and reducing the pressure almost back to $p_0$. During the pressure increase, the AFM tip was secured by retracting it about 500 nm. After reapproaching, it was possible to relocate and manipulate the same nanoparticle, which yielded a friction force identical to the one measured before the pressure increase within typical error margins. Since we found dramatic effects on friction by exposure to air for two weeks, the threshold for contamination induced friction changes must lie within the two investigated limits.

## IV. CONCLUSION AND OUTLOOK

In this paper, we presented experiments that address several of the open issues with respect to the contact area dependence of interfacial friction using the model system of antimony nanoparticles sliding on HOPG. One of the most surprising and intriguing results of our previous experiments[34] was the observation of a "frictional duality" with particles showing either high (i.e., easily detectable) or very low (i.e., below our detection limit) friction.[44] Several additional experimental runs have now solidified the existence of a duality between a low friction and a high friction state for this system. To understand its physical origin, we have systematically analyzed different aspects that potentially might impact the interfacial friction. In particular, the following six findings were presented:

(i) In our earlier experiments,[34] the largest particles that showed low friction were of the order of $A_{\mathrm{contact}}=90\ 000\ \mathrm{nm}^2$. The experiments now revealed the existence of the low friction state for particles considerably larger than that.

(ii) The structure of the particles was re-examined, corroborating earlier reports[34,38,39] of an amorphous-crystalline transition. However, the particle's frictional behavior was found to be unaffected by this transition.

(iii) As the growth process induces large variations in the individual particle shapes (round vs. branched), a possible influence of the morphology on friction was examined, yielding a negative result.

(iv) No dependence of friction on the relative angular orientation between particle and substrate was observed, discounting a mechanism similar to the one observed by Dienwiebel *et al.*[51] that is based on establishing either registry or incommensurability of the sliding lattices by rotation.

(v) Another hypothesis that may explain the duality is based on the existence of mobile molecules in the interface acting as mediators for interface friction.[34] Nevertheless, moderate contamination of the interface by short-term exposure to air with pressures up to $10^{-5}$ mbar did not result in apparent changes of the observed friction.

(vi) To further investigate the effects of contamination and structure, we studied the frictional behavior of oxidized nanoparticles that had previously been kept under ambient conditions for several days. This lead to the disappearance of "vanishing friction" nanoparticles, but particles showing a friction comparable to the preoxidation nonvanishing friction level were still found, which suggests that the particle-substrate interface of these particles was unaffected by the oxidization. Other nanoparticles, however, exhibited a tenfold increase in friction, which points toward a full oxidization of the interface.

Despite the above new findings, we are still not yet in a position to unambiguously determine which effects are ultimately responsible for the occurrence of the frictional duality, establishing the need for continuous examination of the subject. Examples of promising future directions are, e.g., (i) experiments where contamination is added on an ongoing basis and over a long period of time while the friction is continuously recorded. This could yield insight into the nature of the transition from low-friction to high-friction states. (ii) Temperature-dependent measurements similar to the ones performed in Refs. 52–54 might also help to identify the role of the hypothetical mobile dirt particles, since low temperatures should freeze such particles, causing changes in friction. (iii) The low-friction state itself deserves more attention, and respective experiments clearly require an increase in measuring sensitivity. If in fact a quantification of the actual friction experienced by a "superlubric" particle could be achieved, its contact area dependence would further shed light on the underlying atomic origins that cause the manifestation of this remarkable low-friction state. (iv) Finally, the analysis of other material combinations might clarify whether the duality observed for antimony on HOPG is a general effect or if it appears to be particular to the Sb/HOPG system.

## ACKNOWLEDGMENTS

Financial support was provided by the DFG (Grant No. SCHI 619/8-1), the EUROCORES program FANAS of the European Science Foundation (CRP Nanoparma), and the EC sixth framework program (Grant No. ERAS-CT-2003-980409). Work at Yale was supported by the National Science Foundation (Grant No. MRSEC DMR 0520495). C.R. acknowledges the receipt of a personal stipend by the DFG.

*schirmeisen@uni-muenster.de

[1] B. Bhushan, J. N. Israelachvili, and U. Landmann, Nature (London) **374**, 607 (1995).
[2] C. M. Mate, G. M. McClelland, R. Erlandsson, and S. Chiang, Phys. Rev. Lett. **59**, 1942 (1987).
[3] G. Binnig, C. F. Quate, and Ch. Gerber, Phys. Rev. Lett. **56**, 930 (1986).
[4] E. Meyer, L. Howald, R. Lüthi, D. Brodbeck, H. Haefke, J. Frommer, and H.-J. Güntherodt, Ultramicroscopy **42-44**, 274 (1992).
[5] L. Howald, R. Lüthi, E. Meyer, G. Gerth, H. Haefke, R. Overney, and H.-J. Güntherodt, J. Vac. Sci. Technol. B **12**, 2227 (1994).
[6] H. Hölscher, A. Schirmeisen, and U. D. Schwarz, Philos. Trans. R. Soc. London, Ser. A **366**, 1383 (2008).
[7] E. Gnecco, R. Bennewitz, T. Gyalog, Ch. Loppacher, M. Bammerlin, E. Meyer, and H.-J. Güntherodt, Phys. Rev. Lett. **84**, 1172 (2000).
[8] A. Schirmeisen, L. Jansen, and H. Fuchs, Phys. Rev. B **71**, 245403 (2005).
[9] M. Evstigneev, A. Schirmeisen, L. Jansen, H. Fuchs, and P. Reimann, Phys. Rev. Lett. **97**, 240601 (2006).
[10] A. Socoliuc, R. Bennewitz, E. Gnecco, and E. Meyer, Phys. Rev. Lett. **92**, 134301 (2004).
[11] A. Socoliuc, E. Gnecco, S. Maier, O. Pfeiffer, A. Baratoff, R. Bennewitz, and E. Meyer, Science **313**, 207 (2006).
[12] U. D. Schwarz, O. Zwörner, P. Köster, and R. Wiesendanger, Phys. Rev. B **56**, 6987 (1997).
[13] U. D. Schwarz, O. Zwörner, P. Köster, and R. Wiesendanger, Phys. Rev. B **56**, 6997 (1997).
[14] H. Hertz, J. Reine Angew. Math. **92**, 156 (1881).
[15] K. L. Johnson, K. Kendall, and A. D. Roberts, Proc. R. Soc. London, Ser. A **324**, 301 (1971).
[16] B. V. Derjaguin, V. M. Muller, and Y. P. Toporov, J. Colloid Interface Sci. **53**, 314 (1975).
[17] U. D. Schwarz, J. Colloid Interface Sci. **261**, 99 (2003).
[18] M. Enachescu, R. J. A. van den Oetelaar, R. W. Carpick, D. F. Ogletree, C. F. J. Flipse, and M. Salmeron, Phys. Rev. Lett. **81**, 1877 (1998).
[19] I. Szlufarska, M. Chandross, and R. W. Carpick, J. Phys. D **41**, 123001 (2008).
[20] T. Junno, K. Deppert, L. Montelius, and L. Samuelson, Appl. Phys. Lett. **66**, 3627 (1995).
[21] L. Theil Hansen, A. Kühle, A. H. Sorensen, J. Bohr, and P. E. Lindelof, Nanotechnology **9**, 337 (1998).
[22] T. Junno, S.-B. Carlsson, H. Xu, L. Montelius, and L. Samuel-

son, Appl. Phys. Lett. **72**, 548 (1998).
[23] H. Xie, D. S. Haliyo, and S. Regnier, Appl. Phys. Lett. **94**, 153106 (2009).
[24] M. R. Falvo, R. M. Taylor II, A. Helser, V. Chi, F. P. Brooks, Jr., S. Washburn, and R. Superfine, Nature (London) **397**, 236 (1999).
[25] M. R. Falvo, J. Steele, R. M. Taylor II, and R. Superfine, Phys. Rev. B **62**, R10665 (2000).
[26] M. Heyde, B. Capella, H. Sturm, C. Ritter, and K. Rademann, Surf. Sci. **476**, 54 (2001).
[27] C. Ritter, M. Heyde, U. D. Schwarz, and K. Rademann, Langmuir **18**, 7798 (2002).
[28] K. Mougin, E. Gnecco, A. Rao, M. T. Cuberes, S. Jayaraman, E. W. McFarland, H. Haidara, and E. Meyer, Langmuir **24**, 1577 (2008).
[29] A. Rao, E. Gnecco, D. Marchetto, K. Mougin, M. Schönenberger, S. Valeri, and E. Meyer, Nanotechnology **20**, 115706 (2009).
[30] A. Schirmeisen and U. D. Schwarz, ChemPhysChem **10**, 2373 (2009).
[31] R. Lüthi, E. Meyer, H. Haefke, L. Howald, W. Gutmannsbauer, and H.-J. Güntherodt, Science **266**, 1979 (1994).
[32] C. Ritter, M. Heyde, B. Stegemann, K. Rademann, and U. D. Schwarz, Phys. Rev. B **71**, 085405 (2005).
[33] P. E. Sheehan and C. M. Lieber, Science **272**, 1158 (1996).
[34] D. Dietzel, C. Ritter, T. Mönninghoff, H. Fuchs, A. Schirmeisen, and U. D. Schwarz, Phys. Rev. Lett. **101**, 125505 (2008).
[35] M. Palacio and B. Bhushan, Nanotechnology **19**, 315710 (2008).
[36] D. Dietzel, M. Feldmann, U. D. Schwarz, H. Fuchs, and A. Schirmeisen, Appl. Phys. Lett. **95**, 053104 (2009).
[37] D. Dietzel, T. Mönninghoff, L. Jansen, H. Fuchs, C. Ritter, U. D. Schwarz, and A. Schirmeisen, J. Appl. Phys. **102**, 084306 (2007).
[38] B. Stegemann, C. Ritter, B. Kaiser, and K. Rademann, J. Phys. Chem. B **108**, 14292 (2004).
[39] B. Kaiser, B. Stegemann, H. Kaukel, and K. Rademann, Surf. Sci. **496**, L18 (2002).
[40] C. S. Barrett, P. Cucka, and K. Haefner, Acta Crystallogr. **16**, 451 (1963).
[41] S. S. Kushvaha, Z. Yan, W. Xiao, and X.-S. Wang, J. Phys.: Condens. Matter **18**, 3425 (2006).
[42] M. Varenberg, I. Etsion, and G. Halperin, Rev. Sci. Instrum. **74**, 3362 (2003).
[43] C. Ritter, B. Stegemann, A. Schirmeisen, and U. D. Schwarz (unpublished).
[44] Note that in this context, the terms "frictionless" and "vanishing friction" only denote a frictional force below our current detection limit and should not imply that there is actually no friction whatsoever. Steps towards an improvement in our measurement sensitivity are currently undertaken that may allow a better quantification of this apparent "superlubric" behavior in the future.
[45] G. He, M. H. Müser, and M. O. Robbins, Science **284**, 1650 (1999).
[46] M. H. Müser, L. Wenning, and M. O. Robbins, Phys. Rev. Lett. **86**, 1295 (2001).
[47] M. H. Müser, Phys. Rev. Lett. **89**, 224301 (2002).
[48] M. H. Müser, EPL **66**, 97 (2004).
[49] Note that the number of particles translated was limited ($n$=7).
[50] S. A. Scott and S. A. Bown, Eur. Phys. J. D **39**, 433 (2006).
[51] M. Dienwiebel, G. S. Verhoeven, N. Pradeep, J. W. M. Frenken, J. A. Heimberg, and H. W. Zandbergen, Phys. Rev. Lett. **92**, 126101 (2004).
[52] A. Schirmeisen, L. Jansen, H. Hölscher, and H. Fuchs, Appl. Phys. Lett. **88**, 123108 (2006).
[53] L. Jansen, A. Schirmeisen, J. L. Hedrick, M. A. Lantz, A. Knoll, R. Cannara, and B. Gotsmann, Phys. Rev. Lett. **102**, 236101 (2009).
[54] I. Barel, M. Urbakh, L. Jansen, and A. Schirmeisen, Phys. Rev. Lett. **104**, 066104 (2010).